Iranian Journal of Geophysics, Vol 19 No 3, 2025, Page 63 – 76 (Research Article)
DOI: 10.30499/ijg.2024.434652.1563

Identification of subsurface structures and potential reservoir zones of geothermal filds based on gravitr data analysis in the Karaha-Cakrana area, west Java

Salma Azmi Nabila Rahman[1], Agustya Adi Martha [2], Sutrisno Sutrisno [3], Amara Wulandari[4] and Nurul Hudayat[5*]

[1] *B.Sc., Physics Study Program, State Islamic University Syarif Hidayatullah Jakarta, Jakarta, Indonesia*
[2] *Assistant Professor, Research Center for Geospatial - National Research and Innovation Agency, Bogor, Indonesia*
[3] *Assistant Professor, Physics Study Program, State Islamic University Syarif Hidayatullah Jakarta, Jakarta, Indonesia*
[4] *B.Sc., Pro-Tech Engineering Corporation, Cibinong, Bogor Regency, Indonesia*
[5] *M.Sc., Research Center for Geospatial - National Research and Innovation Agency, Bogor, Indonesia*

(Received: 10 January 2024, Accepted: 29 June 2024)

Abstract

The Karaha-Cakrabuana area in West Java is believed to contain geothermal prospects. The discovery of geothermal manifestations in the form of fumaroles and hot springs requires further development for optimal utilization. This research aims to identify subsurface structures and potential reservoir zones using gravity methods. The research data consist of GGMplus satellite gravity data, processed using Geosoft Oasis Montaj software, and modeled using ZondGM2D. The results of the Second Vertical Derivative (SVD) curve analysis indicate the possibility of both thrust and normal faults. The SVD graph analysis reveals the presence of eleven fault structures, including eight assumed variations of uplift fault structures and three variations of normal fault structures. Faults are believed to exist in specific locations in the foothill region of Mount Talaga Bodas, in the vicinity of Mount Talaga Bodas, at the base of Mount Sawal, and in the area of Karaha Crater. The 2D inversion modeling results identify rocks based on density distribution patterns, namely densities of 1.027 gr/cm3 - 1.6 gr/cm3 and densities between -2.06 gr/cm3 - 1.32 gr/cm3, suggesting tuff and lahar rocks. Densities of 1.68 gr/cm3 - 2.01 gr/cm3 and 1.8 gr/cm3 - 3.74 gr/cm3 suggest breccia and tuff rocks. Densities of 2.09 gr/cm3 - 2.18 gr/cm3 and 4.22 gr/cm3 - 4.7 gr/cm3 are indicative of andesite lava.

Keywords: GGMplus, Karaha-Cakrabuana, Gravity Method, Geothermal, Subsurface Structure, Reservoir Zone

*Corresponding author: nurul.hudayat@brin.go.id

1 Introduction

According to information from the Ministry of Energy and Mineral Resources, Indonesia has a geothermal potential of 29.5 GW, which accounts for 40% of the world's geothermal potential. It is located in a subduction zone formed by the convergence of three tectonic plates: the Indo-Australian Plate, the Eurasian Plate, and the Pacific Plate. The subduction zone is responsible for the formation of volcanic arcs that stretch from Sumatra to Java and bend northward from the Maluku Islands to northern Sulawesi. The volcanic mountain ranges found throughout the region are indicators of the presence of these volcanic arcs (Khasmadin and Harmoko, 2021).

Karaha-Cakrabuana in West Java is believed to have geothermal prospects due to the discovery of geothermal manifestations such as solfataras and hot springs. According to the Directorate of Geothermal in 2017, the permit holder for the Karaha-Cakrabuana Geothermal Working Area (WKP) is PT Pertamina Geothermal Energy. The Karaha-Cakrabuana WKP covers an area of 64,510 hectares and is located approximately 26 km north of Tasikmalaya City, West Java (ESDM, 2017).

Geothermal manifestations in the form of solfataras were found in Saat Crater, Talaga Bodas 1 Crater, and Pajagalan Crater. Hot springs were found in Pajagalan Crater and Karaha Crater. Based on resource potential hypotheses, the Talaga Bodas Mountain geothermal potential point is estimated to have a capacity of 75 MWe, with a suspected reserve of 120 MWe, and an estimated proven reserve of 80 MWe. The Karaha Mountain geothermal potential point is estimated to have a capacity of 50 MWe, with a suspected reserve of 70 MWe, an estimated proven reserve of 30 MWe, and a proven reserve of 30 MWe. The Sawal Mountain geothermal potential point is speculated to have a capacity of 25 MWe, and the Cipanas-Ciawi geothermal potential point is speculated to have a capacity of 50 MWe. According to the National General Energy Plan (RUEN), as of 2020, geothermal energy sources have been utilized up to 3,109.5 MW, which accounts for only 10.5% of the total utilized energy potential. To meet the increasing energy demand, PT Pertamina Geothermal Energy has been conducting observations and explorations of the geothermal potential in the Karaha-Cakrabuana Geothermal Working Area (WKP). This work is done as part of the development and utilization of geothermal energy resources. A geothermal power plant with a capacity of 30 MWe was installed in 2017, and another plant with a capacity of 20 MWe was installed in 2022. The main parameters of a geothermal system are typically determined using geophysical methods. The gravity method is one of the geophysical methods that can provide information about subsurface structures and estimate reservoir zones, based on the differences in rock mass density within a research area (Jamaluddin et al., 2019).

Based on the regional geological map of Tasikmalaya City (Budhitrisna, 1986), the research area consists of four rock formations. First, there is the result of ancient volcanic activity (QTv(s,k,b,c,r,d)), which includes volcanic breccia, tuff, and lava ranging from andesite to basalts, believed to originate from Mount Sawal, Mount Kukus, Mount Cakrabuana, Mount Sadakeling, Mount Cereme, and Mount Cikuray. Second, there is the result of recent volcanic activity (Qv(g,u,t)), which includes volcanic breccia, lahars, and tuff ranging from andesite to basalts, believed to originate from Mount Galunggung, MountTalaga Bodas, and Mount Cereme.

Table 1. Stratigraphy of the Research Area [ESDM (2017)].

Age		Rock Units	Description
Geology	**Million Years**		
		Alluvium	Loose material
		Volcanic Breccia VIII (Mt.Haruman)	Breccia (Fragments, Pumice Stone and Andesite)
		Volcanic Breccia VII (Mt.Prongol)	Andesite Lava and Lahar Deposit
		Andesite (Mt.Prongol)	Andesite Lava
Quarter		Tufa (Mt.Putri)	Pyroclastic deposits interbedded with lava
			Andesite Breccia
	0.32	Volcanic Breccia VI(Mt.TalagaBodas)	Andesite Lava
	0.5	Andesite (Mt.Sawal)	Andesite Lava
		Andesite (Mt.Eweranda)	Andesite Lava
		Andesite (Mt.Putri)	Breccia, Tufa and Lava
	0.554	Volcanic BrecciaV(Mt.Putri-Eweranda)	
		Andesite (Mt.Sadakeling)	Andesite Lava
		Volcanic Breccia IV(Mt.TalagaBodas)	Lahar flow, Pyroclastic Deposit, Lava
		Andesite and Breccia (Mt. TalagaBodas)	Andesite Lava and Lahar Breccia
		Tufa (Mt.Talaga Bodas)	Tufa and Pyroclastic Deposit
		Volcanic Breccia III (Mt.Cakrabuana)	Breccia and Andesite Lava
	0.649		
		Volcanic Breccia II (Mt. Cakrabuana)	Breccia, Tufa and Andesite Lava
	1.30		
Tersier	1.74	Volcanic Breccia I (Mt.Sadakeling)	Lahar Deposits and Lava Flow

Third, the Mount Galunggung volcanic breccia (Qvb) consists of volcanic breccia containing fragments of andesite lava. Fourth, the Kaliwangu formation (Tpkw) consists of claystone interbedded with tuffaceous sandstone, conglomerate, limestone, and limestone rocks (Arisbaya et al., 2018).

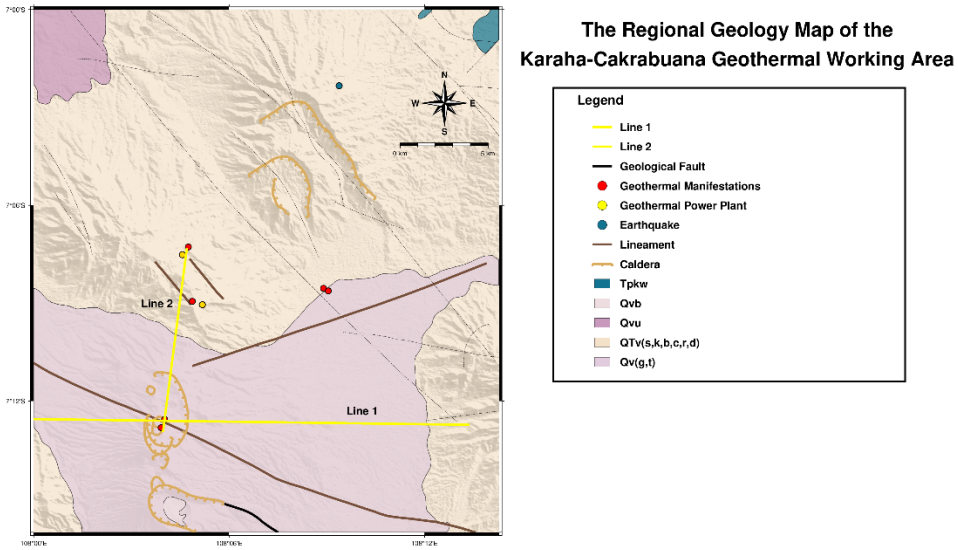

Figure 1. Digitization of the Regional Geological Map of the Karaha-Cakrabuana Geothermal Working Area, West Java by T. Budhitrisna, Ministry of Energy and Mineral Resources, Geological Survey Center.

Geologically, the main prospects in the Karaha-Cakrabuana area consist of Quaternary volcanic rocks such as breccia, andesite, and tuff. Tertiary volcanic rocks (andesite) and diorite intrusions are commonly found in the mountains to the northeast. A geothermal system is the natural transfer of heat with a certain volume flowing to the surface, then to a heat source, and returning to a transmission network, which is typically the Earth's surface (Franco and Donatini, 2017).

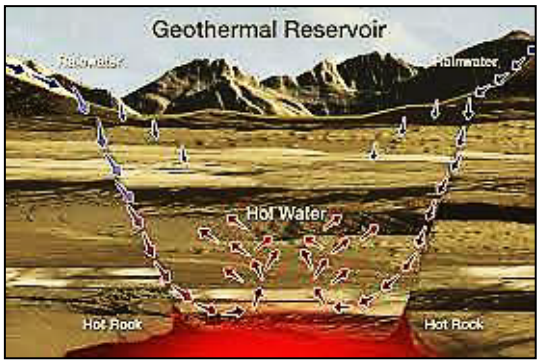

Figure 2. Geothermal System.

In the geological process, there is movement and shifting of tectonic plates, resulting in the formation of faults. In deep locations above the descending plate, there is an increase in temperature, causing the melting of rocks and the formation of magma. Some of the magma moves towards the Earth's crust, while some remains below to heat rocks and water. The heated water rises to the surface through faults and fractures as hot springs or geysers (Csányi et al. 2010).

The hot water that reaches the surface contains trapped steam in permeable rocks, which emerges as surface manifestations such as fumaroles, hot springs, mud pools, and geysers. At the upper part of the heat source, there is a high porosity area covered by low-permeability rocks (caprock), and this area is called a geothermal reservoir (Keam et al. 2005).

Gravity Correction

Free air correction is applied to remove the effect of height h above the Earth's gravitational field by neglecting the mass located between the observation point and the reference spheroid (Jusmi, 2018). The equation for the free air correction is given as equation (1).

$$FAC = \pm(0.3086)h \quad (1)$$

The result of the free air correction is used to calculate the free air anomaly.

$$FAA = g_{obs} - g_{\Phi} + FAC \quad (2)$$

The Bouguer correction is applied to remove the effect of height h above the Earth's gravitational field without neglecting the mass beneath it (Gunawan et al. 2022). The equation for the Bouguer correction is given as equation (3).

$$\Delta g_B = 2\pi G\rho H = \beta\rho H(g.u.) \quad (3)$$

The field correction is applied to remove the mass effect caused by the uneven topography around the observation point (Telford et al. 1990). The equation for the field correction is given as equation (4).

(4)

$$TC = G\rho\theta\left[(r_2 - r_1) + \sqrt{r_1^2 - z^2} - \sqrt{r_2^2 + z^2}\right](g.u.)$$

2 Methods

This research is in the Karaha-Cakrabuana area, West Java. Geographically, it is situated at coordinates (6°59'13.59" S, 107°59'8.94" E), (6°59'20.27" S, 108°13'44.77" E), (7°15'32.79" S, 108°13'51.46" E), (7°15'33.18" S, 107°59'2.18" E).

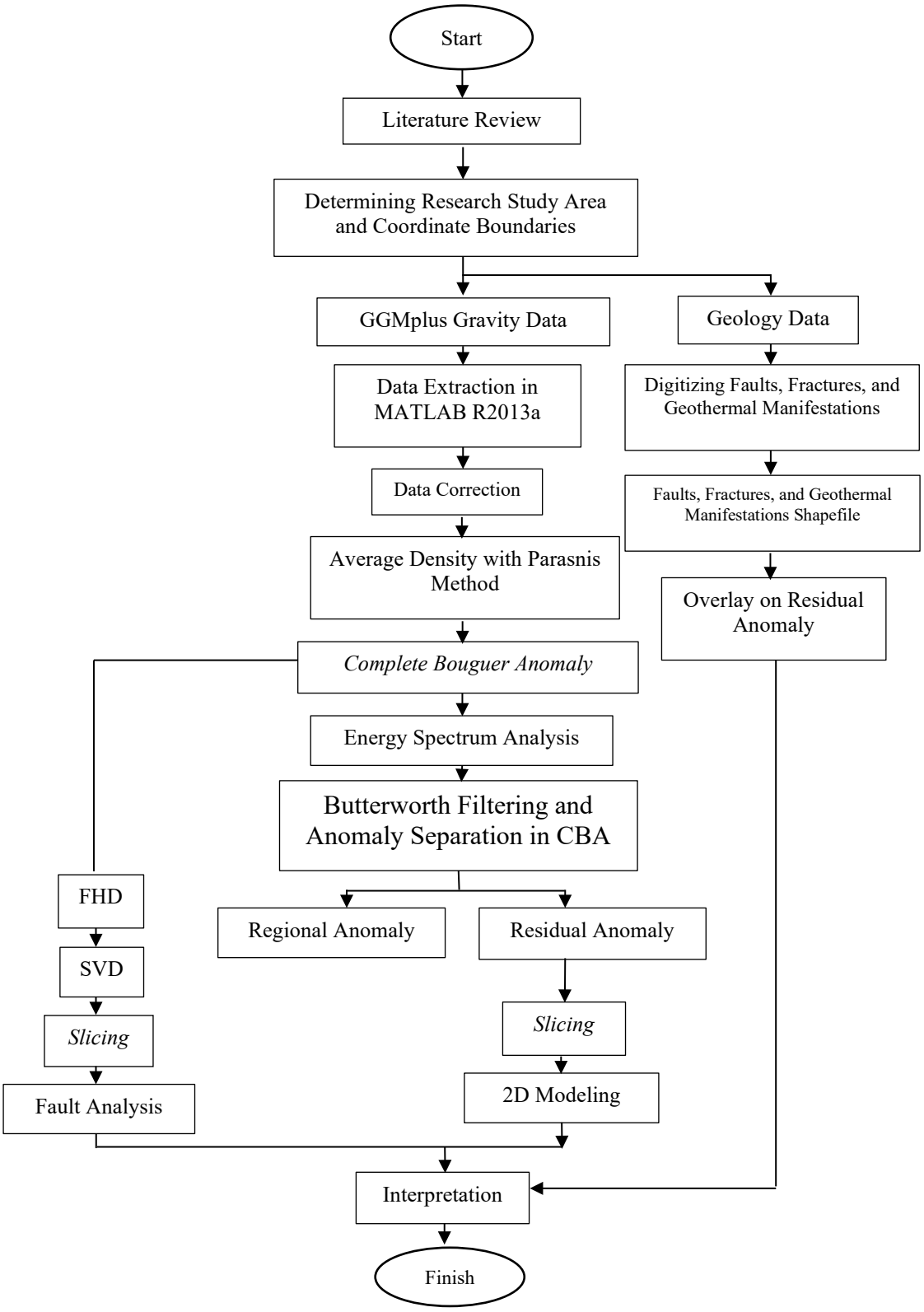

Figure 3. Flowchart of this research

Universal Transverse Mercator (UTM) map projection, World Geodetic System (WGS) 1984, Zone 49S. The research data consists of Global Gravity Model Plus (GGMplus) satellite gravity data with a denser point spacing of 220 meters. GGMplus is a gravity dataset that has been employed in research within the oil and gas industry (Juwita et al. 2024) and fault determination (Martha et al. 2023).

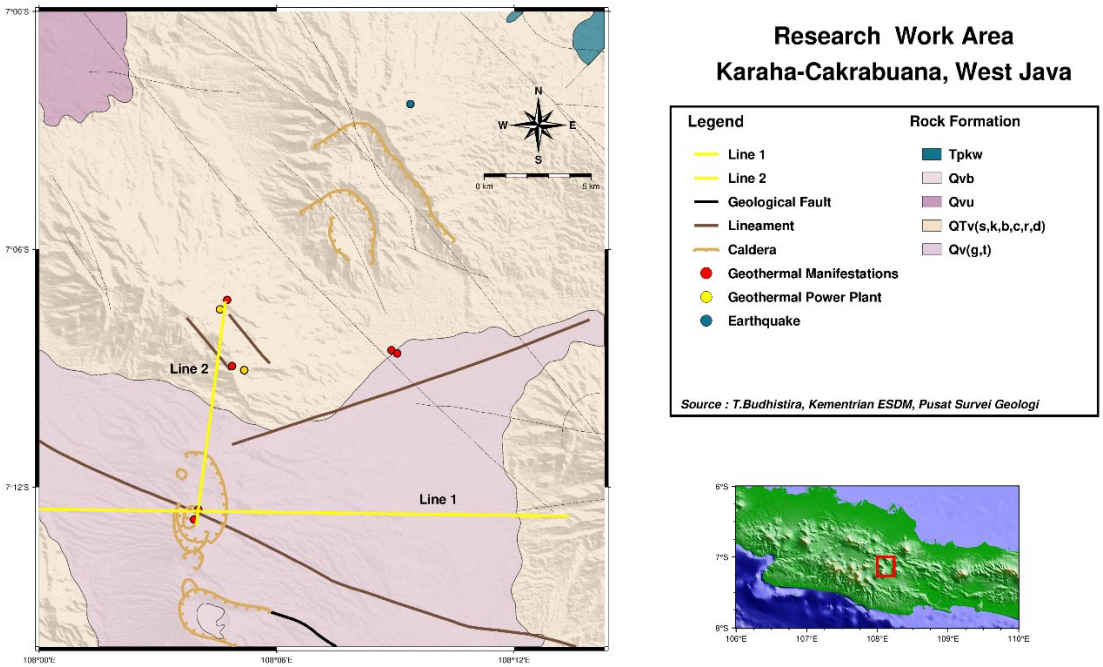

Figure 4. Research Work Area.

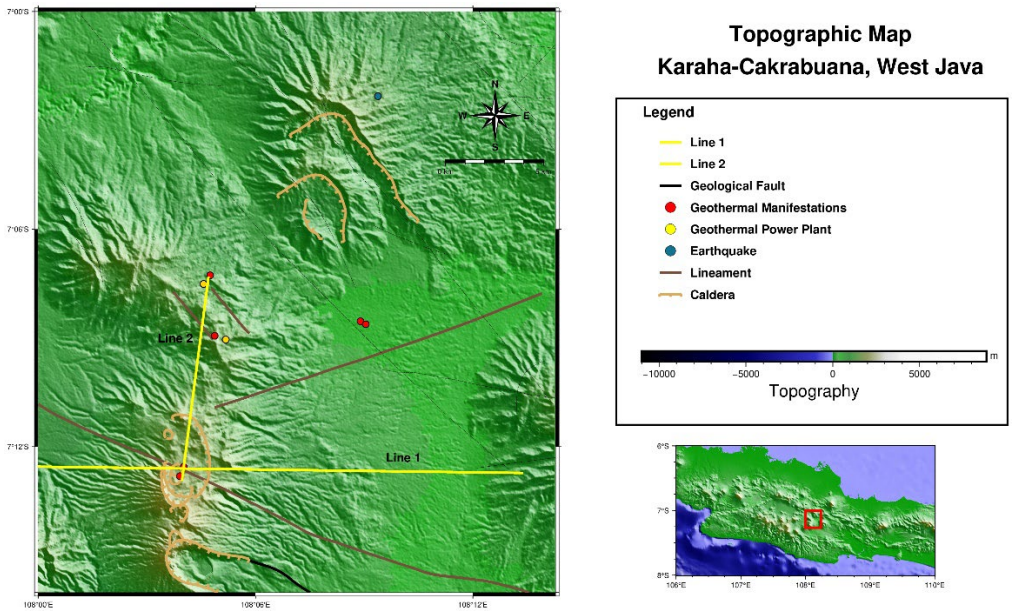

Figure 5. Topographic Map.

The research process is illustrated in the flow diagram in Figure 3. Data was downloaded from this link (https://ddfe.blazejbucha.com/models/GGMplus/data/), then extracted and corrected.

SRTM topography data with a grid spacing of 1 arc sec or 30 m was used to calculate terrain correction (Figure 5).

Average density values and Complete Bouguer Anomaly (CBA) were obtained. CBA was derived into FHD and SVD, with SVD being cut to analyze fractures. Additionally, CBA was utilized to separate anomalies into regional and residual categories. Residual anomalies were then used for 2D inversion modeling using ZondGM2D to identify subsurface structures and predict reservoir zones. Interpretation and correlation were performed with geological data from the research area.

3 Results and Discussion

3.1 Complete Bouger Anomaly

The complete Bouguer anomaly is caused by variations in rock density values from the surface to a certain depth. High values of the complete Bouguer anomaly indicate rock structures with high density, while low values suggest rock structures with low density. The map of complete Bouguer anomaly with a density of 2.5 g/cm³ in Figure 6 shows anomaly values ranging from 37.85 mGal to 73.99 mGal.

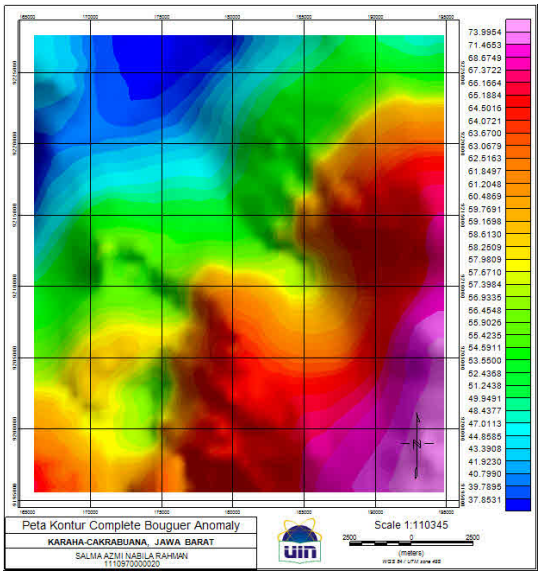

Figure 6. Contour Map of CBA.

The anomalies are categorized into three types: low anomalies, ranging from 37.85 mGal to 48.4 mGal, are predominantly found in the northwest direction, represented by shades of dark blue to light blue. Moderate anomalies, ranging from 49.95 mGal to 63.067 mGal, are oriented in the northeast, west, and southwest with shades of green to orange. High anomalies, ranging from 63.67 mGal to 73.99 mGal, are concentrated in the east, southeast, south, and southwest, depicted with shades of red to light purple. The pattern of high anomalies based on the regional lithology of Karaha-Cakrabuana is caused by rocks of Young Volcanic Products (Qv(g,t)), rocks of Old Volcanic Products (QTv(s,k,b,d)), and the Breccia of Mount Galunggung Volcano. The pattern of low anomalies based on the regional lithology of Karaha-Cakrabuana is caused by rocks of Young Volcanic Products (Qvu) and rocks of Old Volcanic Products (QTv(b,d)). The map of the complete Bouguer anomaly in Figure 7 (a) was created by the Geological Research and Development Center using US topographic maps. The locations of gravity measurement points and elevations were determined from the basic Earth shape map. Based on both maps of the complete Bouguer anomaly, it is evident that the map of the complete Bouguer anomaly with a density of 2.67 g/cm³ from GGMplus data (Figure 7(b)) appears denser than the digitized map of the Bouguer anomaly (Figure 7(a)), due to the tighter spacing of points in the GGMplus data (approximately 220 meters apart).

3.2 Regional and Residual

Regional anomalies and residual anomalies overlap due to their interaction, so these anomalies are separated using a Butterworth filter.

The contour map of regional anomalies has a wide and regular distribution because the effects of subsurface rocks are more homogeneous, resulting in smoother contours. Regional anomaly values, shown in Figure 8(a), range from 38.4 mGal to 73.6 mGal. The contour map of

residual anomalies has a rough and closed contour pattern due to the distribution of shallow rock density (near the surface). Residual anomaly values in Figure 8 (b) range from -1.25 mGal to 1.79 mGal.

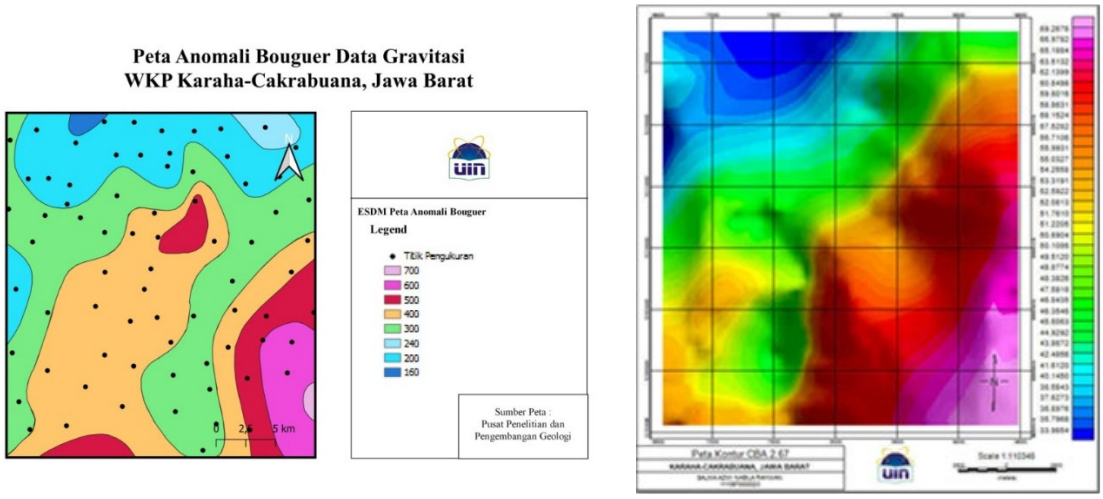

(a) (b)

Figure 7. (a) Digitization of the CBA Map of the Karaha-Cakrabuana Geothermal Working Area (WKP) in West Java by the Geological Research and Development Center. (b) Contour Map of CBA (Complete Bouguer Anomaly) with a Density of 2.67 g/cm³.

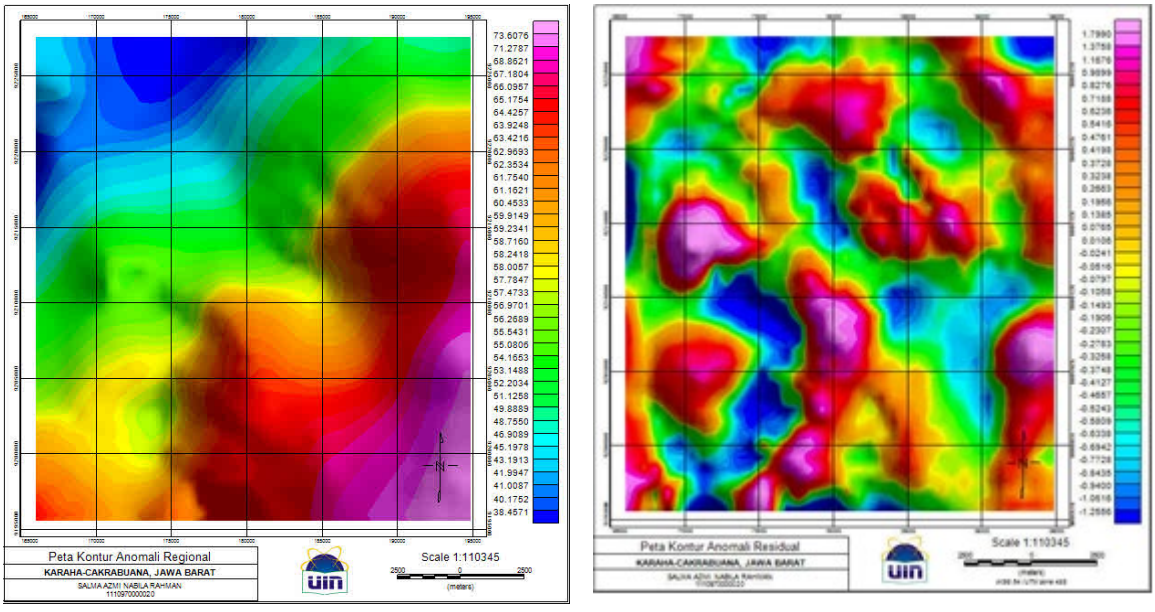

(a) (b)

Figure 8. (a) Contour Map of Regional Anomalies (b) Contour Map of Residual Anomalies

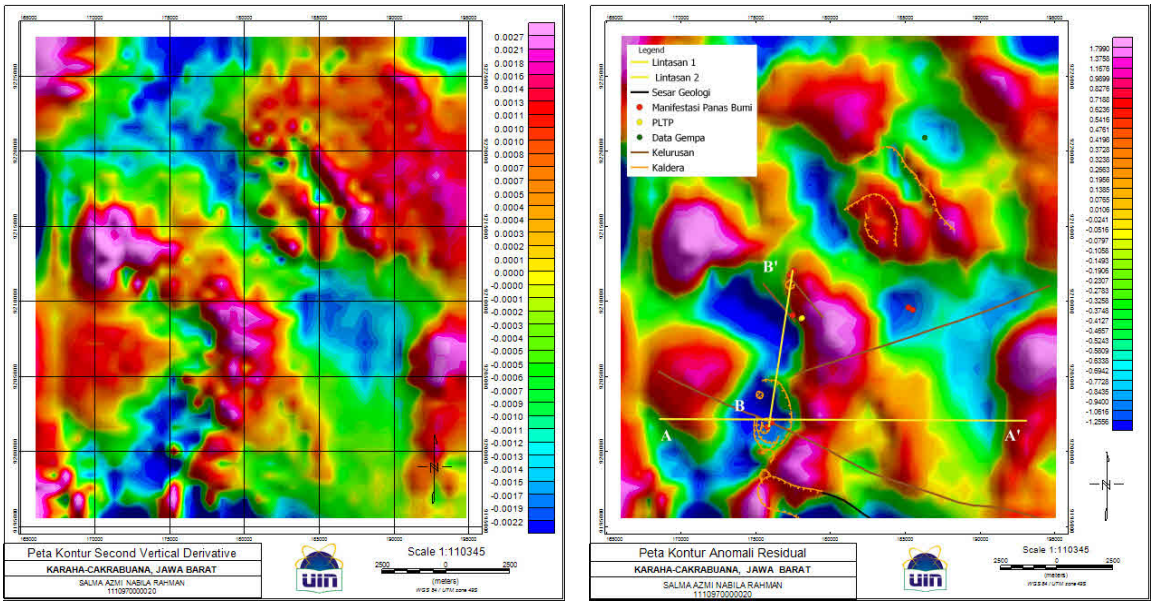

(a) *(b)*

Figure 9. (a) Contour Map of Second Vertical Derivative (b) Digitized Slice Map of Residual Anomalies.

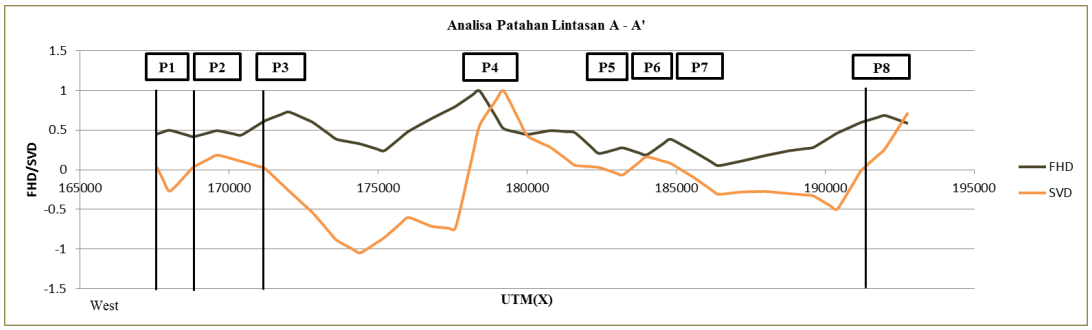

Figure 10. Graph of FHD and SVD along Profile A-A'.

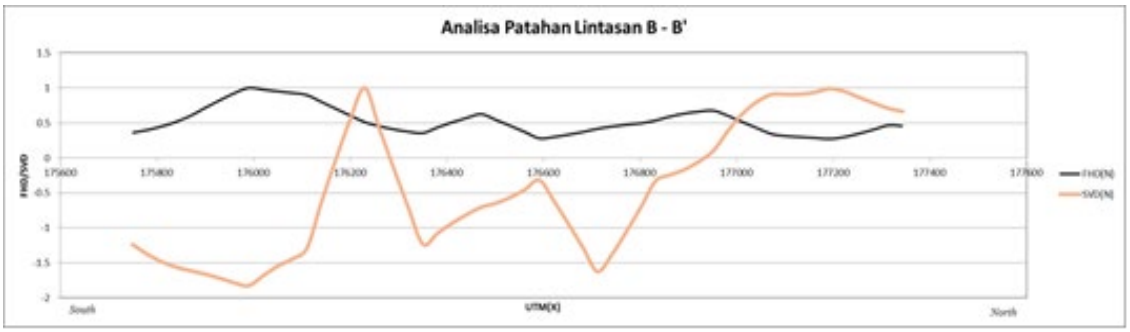

Figure 11. Graph of FHD and SVD along Profile B-B'.

3.3 Second Vertical Derivative (SVD)

The SVD method provides information about the presence of fault structures. The contrast in density between high and low anomalies at short distances indicates fault structures. In the SVD method, the boundary of fault structures is limited by values close to zero or exactly zero, is known to emphasize information from zero anomalies contained in gravity data, as a value of 0 mGal/m² indicates lateral density contrast indicative of faults. Anomalies obtained from geological structures show absolute maximum and minimum values. The criteria for determining the types of faults are presented as follows (Reynolds, 1997):

$$|SVD|min < |SVD|max = Normal\ Fault$$
$$|SVD|min > |SVD|max = Thrust\ Fault$$

These criteria have been utilized in research on detecting types of faults (Sastranegara et al., 2015; Wahyudi et al., 2017; Justia et al., 2018; Hafidah et al., 2019; Alam, 2020; Abiyudo et al., 2021; Ikhwandi et al., 2023).

Profile A-A' in Figure 10 has eight fault structures. The presence of fault structures is determined based on UTM coordinates: P1 with coordinates 167569.5 UTM (x) and 9202118.9 UTM (y), P2 with coordinates 168769.5 UTM (x) and 9202122 UTM (y), P3 with coordinates 171169.5 UTM (x) and 9202128.1 UTM (y), P4 with coordinates 178169.4 UTM (x) and 9202145.8 UTM (y), P5 with coordinates 182569.4 UTM (x) and 9202157 UTM (y), P6 with coordinates 183569.4 UTM (x) and 9202159.5 UTM (y), P7 with coordinates 184969.4 UTM (x) and 9202163.1 UTM (y), P8 with coordinates 191369.4 UTM (x) and 9202179.3 UTM (y) on the FHD and SVD graphs.

The type of fault structure P1 is suspected to be a thrust fault, with the absolute minimum SVD value being 0.2641 mGal/m², which is more than the absolute maximum SVD value of 0.0343 mGal/m². The type of fault structure P2 is suspected to be a thrust fault, with the absolute minimum SVD value being 0.2641 mGal/m², which is more than the absolute maximum SVD value of 0.1464 mGal/m². The type of fault structure P3 is suspected to be a thrust fault, with the absolute minimum SVD value being 0.4611 mGal/m², which is more than the absolute maximum SVD value of 0.0448 mGal/m². The type of fault structure P4 is suspected to be a normal fault, with the absolute minimum SVD value being 0.7370 mGal/m², which is less than the absolute maximum SVD value of 0.8901 mGal/m². The type of fault structure P5 is suspected to be a thrust fault, with the absolute minimum SVD value being 0.0407 mGal/m², which is more than the absolute maximum SVD value of 0.0383 mGal/m². The type of fault structure P6 is suspected to be a normal fault, with the absolute minimum SVD value being 0.0407 mGal/m², which is less than the absolute maximum SVD value of 0.1609 mGal/m². The type of fault structure P7 is suspected to be a thrust fault, with the absolute minimum SVD value being 0.3037 mGal/m², which is more than the absolute maximum SVD value of 0.1089 mGal/m². The type of fault structure P8 is suspected to be a thrust fault, with the absolute minimum SVD value being 0.1181 mGal/m², which is more than the absolute maximum SVD value of 0.0247 mGal/m².

Profile B-B' in Figure 11 has three fault structures. The presence of fault structures is determined based on UTM coordinates: P9 with coordinates 176200.2 UTM (x) and 9204618.8 UTM (y), P10 with coordinates 176260.4 UTM (x) and 9205014.2 UTM (y), and P11 with coordinates 176952.4 UTM (x) and 9209561.8 UTM (y) on the FHD and SVD graphs. The type of fault structure P9 is suspected to be a thrust fault, with the absolute minimum SVD value being 1.294

mGal/m², which is more than the absolute maximum SVD value of 1 mGal/m². The type of fault structure P10 is suspected to be a thrust fault, with the absolute minimum SVD value being 1.234 mGal/m², which is more than the absolute maximum SVD value of 1 mGal/m². The type of fault structure P11 is suspected to be a normal fault, with the absolute minimum SVD value being 0.329 mGal/m², which is less than the absolute maximum SVD value of 0.908 mGal/m².

From the analysis of the SVD graph, the presence and types of fault structures are identified and plotted on the SVD contour map using UTM coordinate data, revealing the location of the fault structures.

Plotting the presence of fault structures based on UTM coordinates in Figure 11, namely P1, P2, P3, P5, P6, and P7, is suspected to be in the foothills of Mount Talaga Bodas. P4, P9, and P10 are suspected to be in the area of Mount Talaga Bodas. P8 is suspected to be in the foothills of Mount Sawal, and P11 is suspected to be in the area of Karaha Crater. The fault structures correlate well with the literature due to the observation of patterns of high and low anomalies occurring at short distances.

3.4 Modeling Analysis

2D modeling is conducted to provide information on subsurface structures in the research area, specifically the distribution of subsurface rocks based on rock density. The 2D modeling utilizes residual anomalies along two profiles, namely A-A' and B-B', using the ZondGM2D software, inputting longitude, latitude, and gravity observation data. The inversion process involves adjusting the number of cells influencing resolution and depth. The inversion is carried out twice until a satisfactory match between observations and measurements is achieved. The result is a 2D inversion model that approximates the actual subsurface structure.

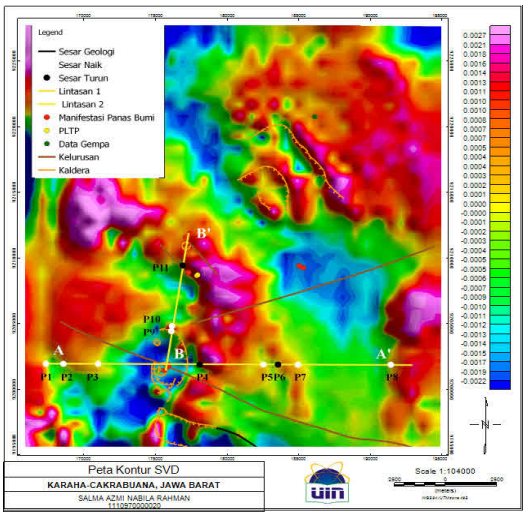

Figure 12. Fault Plot on SVD Contour Map.

2D Inversion Modeling for Profile A-A' in Figure 12 is oriented from west to east, with density values ranging from 1.027 g/cm³ to 2.18 g/cm³, elevations at approximately 1500 meters, and depths ranging from -3000 meters. Density values between 1.027 g/cm³ and 1.6 g/cm³ are suspected to represent Young Volcanic Products (Qvt) rocks formed during the mid-lower Holocene and uppermost Pleistocene, consisting of tuff and volcanic mudflow rocks.

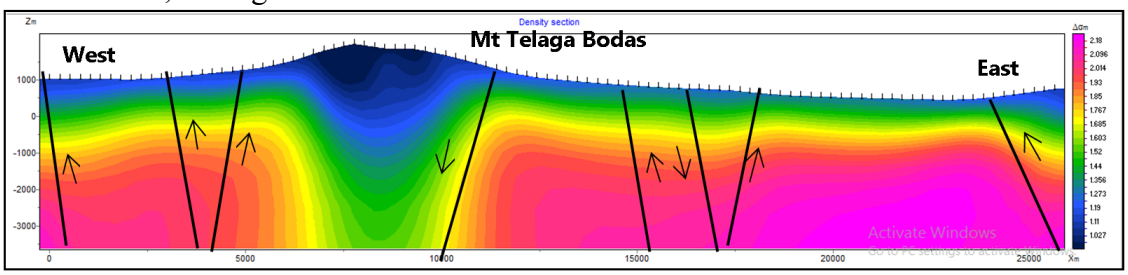

Figure 13. 2D Inversion Modeling for Profile A-A'.

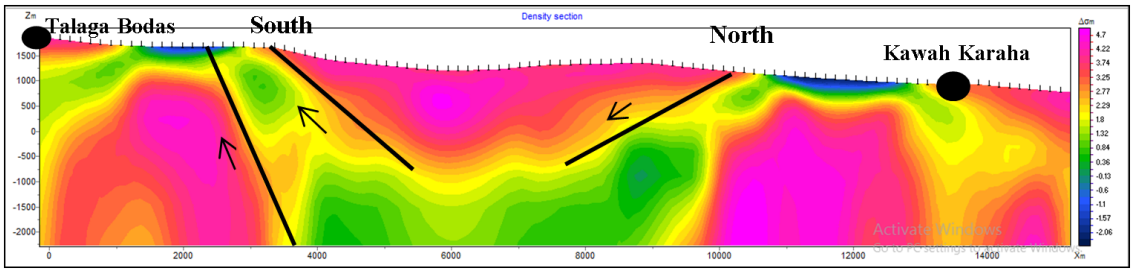

Figure14. 2D Inversion Modeling for Profile B-B'.

Density values between 1.68 g/cm³ and 2.01 g/cm³ are suspected to represent Old Volcanic Products (QTv(s,k)) rocks formed during the mid-lower Pleistocene, consisting of breccia and tuff rocks. Density values between 2.09 g/cm³ and 2.18 g/cm³ are suspected to represent Old Volcanic Products (QTv(s,k)) rocks formed during the mid-lower Pleistocene, consisting of andesitic lava as a heat source. 2D Inversion Modeling for Profile B-B' in Figure 13 is oriented from south to north, with density values ranging from -2.06 g/cm³ to 4.7 g/cm³, elevations at approximately 1500 meters, and depths ranging from -2000 meters.

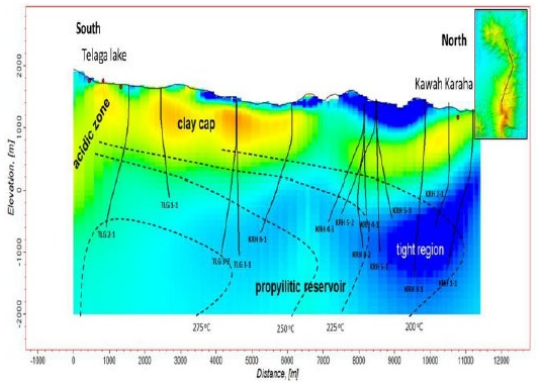

Figure 15. MT Resistivity Model from the Geothermal Potential Book by EBTKE.

Density values between -2.06 g/cm³ and 1.32 g/cm³ are suspected to represent Young Volcanic Products (Qvt) rocks formed during the mid-lower Holocene and uppermost Pleistocene, consisting of tuff and volcanic mudflow rocks. Density values between 1.8 g/cm³ and 3.74 g/cm³ are suspected to represent Old Volcanic Products (QTvd) rocks formed during the mid-lower Pleistocene, consisting of breccia and tuff rocks. Density values between 4.22 g/cm³ and 4.7 g/cm³ are suspected to represent Old Volcanic Products (QTvd) rocks formed during the mid-lower Pleistocene, consisting of andesitic lava, presumed to be a source of heat.

The MT resistivity model in Figure 15 is compared with the 2D gravity inversion model in Figure 14 along the same profile, namely Profile B-B'. Both models have elevation values ranging from around 2000 meters and depth values ranging from -2000 meters. The comparative results indicate congruence between the MT model and the 2D gravity inversion model in this study. In this research, the basement rock is known to have an inverse relationship between gravity density and MT resistivity. In the MT resistivity modeling, the basement rock is marked in blue, while the overlying rock is marked in red. On the other hand, in the 2D gravity inversion modeling, the basement rock is marked in red, and the overlying rock is marked in blue. The basement rock is associated with high gravity anomalies, while the overlying rock is associated with low gravity anomalies.

5 Conclusions

Based on the conducted research, the following conclusions can be drawn:

1. Based on the analysis of the SVD graph, there are eleven fault structures with a presumed eight types of uplift fault structures and three types of normal fault structures. The presence of faults based on UTM coordinates, namely P1, P2, P3, P5, P6, and P7, is suspected to be in the foothill area of Mount Talaga Bodas. P4, P9, and P10 are suspected to be in the area of Mount Talaga Bodas. P8 is suspected to be at

the base of Mount Sawal, and P11 is suspected to be in the area of Karaha Crater.

2. Based on the 2D inversion model, Profile A-A' has density values ranging from 1.027 g/cm³ to 1.6 g/cm³, suspected to be Young Volcanic Products (Qvt) in the form of tuff and volcanic mudflow rocks. Density values ranging from 1.68 g/cm³ to 2.01 g/cm³ are suspected to be Old Volcanic Products (QTv(s,k)) in the form of breccia and tuff rocks. Density values ranging from 2.09 g/cm³ to 2.18 g/cm³ are suspected to be Old Volcanic Products (QTv(s,k)) in the form of andesitic lava. On the other hand, Profile B-B' has density values ranging from -2.06 g/cm³ to 1.32 g/cm³, suspected to be Young Volcanic Products (Qvt) in the form of tuff and volcanic mudflow rocks. Density values ranging from 1.8 g/cm³ to 3.74 g/cm³ are suspected to be Old Volcanic Products (QTvd) in the form of breccia and tuff rocks. Density values ranging from 4.22 g/cm³ to 4.7 g/cm³ are suspected to be Old Volcanic Products (QTvd) in the form of andesitic lava.
3. Based on the inversion model, density values ranging from -0.04 to -0.025 g/cm³ indicate three potential reservoir zones located in Karaha Crater, Mount Talaga Bodas, and near Mount Talaga Bodas.

References

Alam, S. (2020). Stratigraphy and structural pattern of Kebumen Region using second vertical derivative of gravity data, Central Java. Journal of Geological Sciences and Applied Geology, 4(1), 27.

Abiduyo, R., Daud, Y., & Satya, D.S. (2021). Subsurface Structure Identification from Gravity Modelling of Silangkitang Geothermal Field for Future Injection Well Targeting. PROCEEDINGS, The 2nd Digital Indonesia International Geothermal Convention (DIIGC) 2021

Aldinofrizal, A., Arisbaya, I., Gaffar, E. Z., Harja, A., & Sudrajat, Y. (2018). Model of the Karaha - Talaga Bodas Geothermal Field Based on 2D Inversion of Magnetotelluric Data. Journal of Geology and Mining Research, 28(2), 221. doi: 10.14203/risetgeotam2018.v28.989.

Armada, M. I., Musa, M. D. T., Maskur, & Badaruddin. (2018). Identification of Subsurface Heat Flow in Lemba Harapan Village, Tolitoli Regency Using Geoelectric Method. Gravitasi, 17(2). doi: 10.22487/gravitasi.v17i2.12422.

Csányi, Ľ., Katin, M., Krištof, V., Kušnír, S., & Marci, M. (2010). Geothermal Energy. Dspacebat University of West Bohemia, 21–25.

Directorate of Geothermal. (2017). Geothermal Potential of Indonesia Volume 1. Directorate of Geothermal, Directorate General of New, Renewable Energy and Energy Conservation, Ministry of Energy and Mineral Resources (ESDM).

Franco, A., & Donatini, F. (2017). Methods for the Estimation of the Energy Stored in Geothermal Reservoirs. Journal of Physics: Conference Series, 796(1), 012025. doi: 10.1088/1742-6596/796/1/012025.

Gunawan, B., Anjani, A., & Anjalni, A. (2022). Identification of 2D Modeling and Surface Temperature of the Mount Gede-Pangrango Geothermal Area, West Java Using Gravity Method. Journal of Engineering, Environmental, and Energy Sciences, 1(1), 1–14. doi: 10.31599/joes.v1i1.983.

Hafidah, A. D., Daud, Y., & Usman, A.(2019). Reservoir identification based on gravity method at "AUN" geothermal field. E3S Web of Conferences, 125(ICENIS 2019).

Ikhwandi, A. F. F. P. F. L., Arif Ismul Hadi, Hilmi Zakariya, & Refrizon, R. (2023). Identification of the Manna Segment Sumatran Fault Using GGMplus Gravity Anomaly Data with the Second Vertical Derivative (SVD) Method. JURNAL ILMU FISIKA, 15(2), 123–136. https://doi.org/10.25077/jif.15.2.123-136.2023

Jamaluddin, J., Maria, M., Ryka, H., & Afifah, R. S. (2019). Subsurface Modeling of Bantar Karet, West Java Using Gravity Method. Journal of Geocelebes, 3(2), 59. doi: 10.20956/geocelebes.v3i2.6689.

Jusmi, F. (2018). Mapping of Complete Bouguer Anomaly and Topography and Determination of Bouguer Density of Rocks in the Pamancalan Geothermal Area. Journal of Dinamics, 09(01), 1–9.

Justia, M., Hiola, M. F. H., & Febryana, N. B. (2018). Gravity anomaly to identify Walanae fault using second vertical derivative method. Journal of Physics: Theories and Applications, 2(1), 34-42. https://doi.org/10.20961/jphystheor-appl.v2i1.29008

Juwita, W., Juventa, J., setiawan, A. M., Martha, A. A., Hudayat, N., & Sutedja, B. (2023). Identification of Potential Hydrocarbons Traps Using the Gravity Method in the Bengkulu Basin. Iranian Journal of Geophysics. doi: 10.30499/ijg.2023.409882.1535.

Keam, R. F., Luketina, K. M., & Pipe, L. Z. (2005). Definition and Listing of Significant Geothermal Feature Types in the Waikato Region. World Geothermal Congress 2005, April, 1-12.

Khasmadin, M. F., & Harmoko, U. (2021). Study of the Potential and Utilization of Geothermal Energy in the Working Area of Patuha Ciwidey Geothermal. Journal of New and Renewable Energy, 2(2), 101–113. doi: 10.14710/jebt.2021.11187.

Martha, A. A., Setiawan, A., & Setiadi, T. A. P. (2023). Utilization of Global Gravity Model Plus (GGMPlus) to Identify Fault Structures in Mamasa District, West Sulawesi. AIP Conference Proceedings, 2941(1), 030006. doi: 10.1063/5.0181519.

Reynolds, J. M. (1997). An introduction to applied and environmental geophysics (J. Wiley & Sons (eds.); Edition 1). British Library in Publication Data.

Sastranegara, T., Nainggolan, S.S. and Raharjo, I.B.(2015). The Application of a Triangular Mesh for Gravity Inversion to Reconstruct Subsurface Geological Structures in the Hululais Geothermal Prospect, Bengkulu, Proceedings World Geothermal Congress (2015).

Telford, W. M., Geldart, L. P., & Sheriff, R. E. (2005). Applied Geophysics, 2nd edition. Cambridge: Cambridge University Press. doi: 10.1038/127783a0.

Wahyudi, E. J., Kynantoro, Y., & Alawiyah, S. (2017). Second vertical derivative using 3-D gravity data for fault structure interpretation. Journal of Physics: Conference Series, 877(1), 012039. https://doi.org/10.1088/1742-6596/877/1/012039.